Multimodal fusion analysis of functional, cerebrovascular and structural neuroimaging in healthy ageing subjects

Xulin Liu[1], Lorraine K Tyler[2], Cam-CAN[3], James B Rowe[1,4*], and Kamen A Tsvetanov[1,2*]

[1]Department of Clinical Neurosciences, University of Cambridge, Cambridge, UK
[2]The Centre for Speech, Language and the Brain, Department of Psychology, University of Cambridge, Cambridge, UK
[3]Cambridge Centre for Ageing and Neuroscience (Cam-CAN), MRC Cognition and Brain Sciences Unit, University of Cambridge, Cambridge, UK
[4]MRC Cognition and Brain Sciences Unit, University of Cambridge, Cambridge, UK
*Co-last authors
xl454@cam.ac.uk ORCID 0000-0002-8219-2848
lktyler@csl.psychol.cam.ac.uk
camcan-manager@mrc-cbu.cam.ac.uk
james.rowe@mrc-cbu.cam.ac.uk
kat35@cam.ac.uk ORCID 0000-0002-3178-6363
Correspondence: Xulin Liu, xl454@cam.ac.uk

Data availability statement: Data of the Cambridge Centre for Ageing and Neuroscience (Cam-CAN) study are available via the Cam-CAN's portal. Data and codes that support findings of this study are available upon reasonable request.

Funding statement: The Cam-CAN research was supported by the Biotechnology and Biological Sciences Research Council (grant number BB/H008217/1).This work is supported by the Guarantors of Brain (G101149), the Wellcome Trust (103838), the Medical Research Council (SUAG/051G101400; and SUAG/010 RG91365), European Union's Horizon 2020 (732592) and the Cambridge NIHR Biomedical Research Centre. X.L. is supported by the Cambridge Commonwealth, European and International Trust and the China Scholarship Council.

Conflict of interest disclosure: No conflict of interest.

Ethics approval statement: Ethical approval of the Cam-CAN study was obtained from the Cambridge 2 Research Ethics Committee.

Patient consent statement: Written informed consent was given by all participants

Abstract

Cognitive ageing is a complex process which requires multimodal approach. Neuroimaging can provide insights into brain morphology, functional organization and vascular dynamics. However, most neuroimaging studies of ageing have focused on each imaging modality separately, limiting the understanding of interrelations between processes identified by different modalities and the interpretation of neural correlates of cognitive decline in ageing. Here, we used linked independent component analysis as a data-driven multimodal approach to jointly analyze magnetic resonance imaging of grey matter density, cerebrovascular, and functional network topographies. Neuroimaging and behavioural data (n = 215) from the Cambridge Centre for Ageing and Neuroscience study were used, containing healthy subjects aged 18 to 88. In the output components, fusion was found between structural and cerebrovascular topographies in multiple components with cognitive-relevance across the lifespan. A component reflecting global atrophy with regional cerebrovascular changes and a component reflecting right frontoparietal network activity were correlated with fluid intelligence over and above age and gender. No meaningful fusion between functional network topography and structural or cerebrovascular signals was observed. We propose that integrating multiple neuroimaging modalities allows to better characterize brain pattern variability and to differentiate brain changes in healthy ageing.

Keywords: multimodal fusion, linked independent component analysis, neuroimaging, healthy ageing

1. INTRODUCTION

Increasing life expectancy is leading to rapid ageing of the worldwide population (Beard et al., 2016). The quality of these extra years of life heavily depends on good health, including the maintenance of good cognitive function across the lifespan (Beard et al., 2016; Sahakian, 2014). There is a pressing need to better understand the neurobiology of cognitive function associated with ageing. Neuroimaging studies show age-related changes in brain morphology, functional networks, and vascular dynamics (Kennedy & Raz, 2015). However, these effects are usually studied separately, whereas their integration could explain how these components influence cognitive ageing (Tsvetanov, Henson, & Rowe, 2021).

Brain atrophy is one of the most commonly studied features of ageing (Grajauskas et al., 2019; Pini et al., 2016; Romanowski & Wilkinson, 2011). However, atrophy on its own does not fully explain cognitive performance and is insufficient for understanding ageing and neurodegenerative syndromes with heterogenous clinical features (Grajauskas et al., 2019; Murley et al., 2020; Perry et al., 2017; Tsvetanov, Gazzina, et al., 2021; Tsvetanov et al., 2016). Instead, we propose that cognitive ageing is multifactorial, reflecting complex processes which require multivariate techniques to elucidate (Doan, Engvig, Persson, et al., 2017; Doan, Engvig, Zaske, et al., 2017; Douaud et al., 2014; Groves, Beckmann, Smith, & Woolrich, 2011; Murley et al., 2020). Neuroimaging is a key contributor to this approach, from its quantification of brain morphology, functional networks and vascular dynamics.

Brain functional networks are commonly studied using functional magnetic resonance imaging (fMRI), which measures neural activity indirectly via changes in the blood oxygen level-dependent (BOLD) signal (Chen & Glover, 2015; Grady, 2012; Rosen & Savoy, 2012). Cognitive function is dependent on intrinsic interactions within large-scale functional brain networks as well as extrinsic interactions between such functional brain networks (Fox et al., 2005; Kelly, Uddin, Biswal, Castellanos, & Milham, 2008). These networks show selective vulnerability to age and neurodegeneration (Moguilner et al., 2020; Tsvetanov, Gazzina, et al., 2021). Task-free fMRI, also known as resting-state fMRI (rs-fMRI), can be used to characterize intrinsic and

extrinsic connectivity of functional networks simultaneously (Cole, Bassett, Power, Braver, & Petersen, 2014; Smith et al., 2009). Spontaneous activity, which can be measured by rs-fMRI, is the most metabolic demanding component of neural activity (Raichle & Mintun, 2006). Moreover, activities in resting-state functional networks, such as the default mode network (DMN), the salience network (SN) and the frontoparietal network (FPN), are associated with a wide range of cognitive functions (e.g., memory, language, attention, visual processes) (Corbetta & Shulman, 2002) and playing an increasingly important role in maintaining good cognition in old age and progression of some neurodegenerative diseases (Bethlehem et al., 2020; Tibon et al., 2021; Tsvetanov, Gazzina, et al., 2021; Tsvetanov et al., 2016).

Rs-fMRI signals also reflect the haemodynamic response evoked by neuronal activity and therefore fMRI represents both vascular and neuronal signals (Tsvetanov, Henson, & Rowe, 2021). The interpretations of neurocognitive functions from fMRI could be confounded by differences in neurovascular signals associated with normal ageing and other factors (e.g., medications, lifestyle changes) instead of cognitive change. Nevertheless, neurovascular coupling is also implicated as a major factor in maintaining brain health in ageing and neurodegenerative diseases (Iadecola, 2017; Kisler, Nelson, Montagne, & Zlokovic, 2017; Sweeney, Kisler, Montagne, Toga, & Zlokovic, 2018). Dissociation of vascular and neuronal signals would therefore be particularly meaningful (Tsvetanov, Henson, & Rowe, 2021). Consequently, unraveling the interactive effects of changes on morphometry, cerebrovascular and functional levels could provide better understanding of the multifactorial neurobiological mechanisms underlying cognitive change in ageing and neurodegeneration.

The majority of neuroimaging studies have focused on each imaging modality separately, limiting the understanding of interrelations between modalities and the complex neural mechanisms associated with cognitive change. Linked independent component analysis (ICA) is a data-driven analytic method that allows for simultaneous characterization of multimodal imaging modalities while taking into account the co-variance across imaging modalities (Groves et al., 2011). By identifying common patterns that are shared by different imaging modalities

and identifying independent components that are dominated by single imaging modality, one can more accurately characterize the predictors of the outcomes of interest.

We aimed to integrate structural, functional and cerebrovascular neuroimaging signals to better understand cognitive variability. Specifically, we tested whether differences in structural, cerebrovascular, and functional network topography have independent or convergent patterns with age, and whether these patterns are correlated with cognitive function across the lifespan.

2. METHODS

2.1 Cohorts and participants

The Cambridge Centre for Ageing and Neuroscience (Cam-CAN) cohort study recruited healthy adults from its local general population in the UK, in three stages (Shafto et al., 2014). In Stage 1, 3000 adults aged 18 and above were recruited for a home interview. In Stage 2, a subset of 700 participants aged 18-87 (100 per age decile) was selected to participate in neuroimaging (e.g., structural MRI and fMRI) and behavioural tests (Shafto et al., 2014). In Stage 3, a subset of 280 participants (40 per age decile) was selected (referred to as CC280) to participate in further neuroimaging (e.g., fMRI, arterial spin labelling (ASL)) and cognitive examinations across key cognitive domains (Shafto et al., 2014; Taylor et al., 2017). Details of the neuroimaging experiments and cognitive tasks are reported previously (Shafto et al., 2014; Taylor et al., 2017). Ethical approval was obtained from the Cambridge 2 Research Ethics Committee, and written informed consent was given by all participants. Subjects in Cam-CAN Stage 3 (CC280) were analyzed in the main analysis of this study. A subset of Stage 2 that was not included in Stage 3 was analyzed as a validation cohort (details discussed in 2.4).

2.2 Image acquisition and preprocessing

A summary flow chart of the processing and analysis of imaging modalities is presented (**Figure 1**). Details are discussed below.

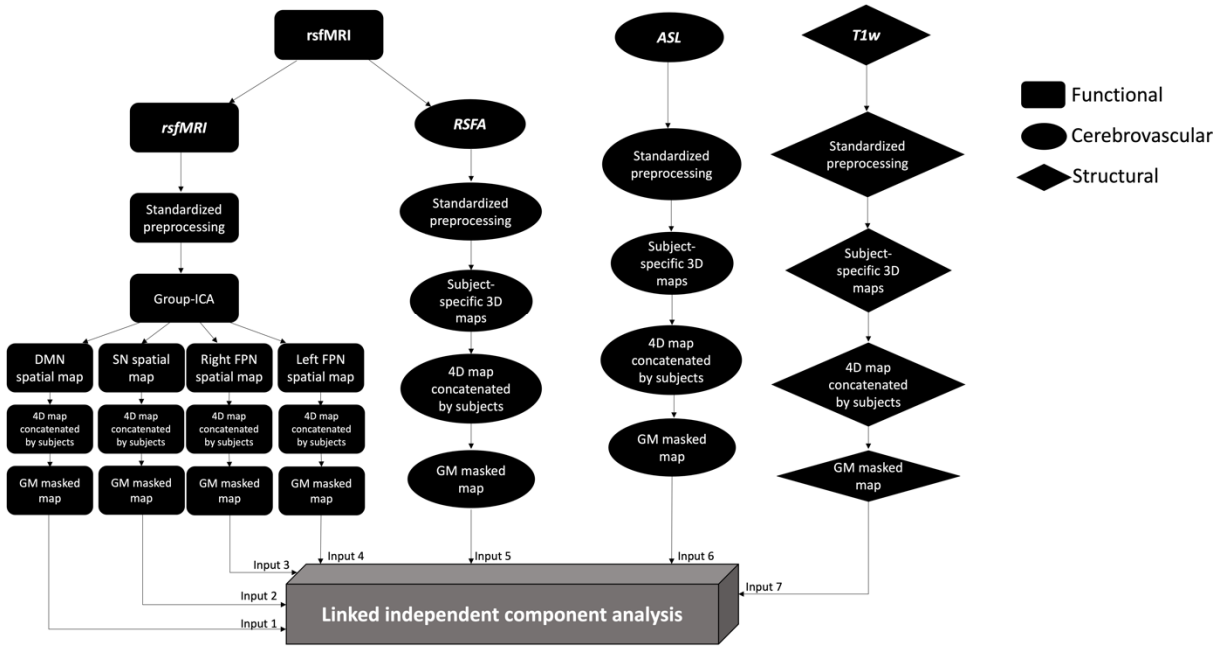

Figure 1. Summary of processing and analysis of the imaging modalities, comprising functional, cerebrovascular and structural measurements. Abbreviations: *ASL*, arterial spin labelling; *DMN*, default mode network; *FPN*, frontoparietal network; *GM*, grey matter; *ICA*, independent component analysis; *RSFA*, resting state fluctuation amplitude; *rsfMRI*, resting-state functional magnetic resonance imaging; *SN*, salience network; T1w, T1-weighted.

2.2.1 T1 structural MRI

Imaging data from Cam-CAN were acquired using a 3T Siemens TIM Trio. A 3D structural MRI was acquired using T1-weighted sequence with generalized autocalibrating partially parallel acquisition with acceleration factor 2; repetition time (TR) = 2250 ms; echo time (TE) = 2.99 ms; inversion time (TI) = 900 ms; flip angle α = 9°; field-of-view (FOV) = 256 X 240 X 192 mm; resolution = 1 mm isotropic; acquisition time of 4 min and 32 s. Preprocessing of T1-weighted images used standardized preprocessing as described elsewhere (Tsvetanov, Henson, Jones, et al., 2021). We used Automatic Analysis (Cusack et al., 2014) pipelines implemented in Matlab (MathWorks). Grey matter images were smoothed with an 8 mm full-width at half maximum (FWHM) Gaussian kernel (Taylor et al., 2017; Tsvetanov et al., 2018). For the linked ICA grey

matter images were down-sampled to match the resolution of fMRI and perfusion data. A brain mask from Statistical Parametric Mapping 12 (SPM12) (https://www.fil.ion.ucl.ac.uk/spm/software/spm12/) was applied at a threshold of 0.9 (i.e., >90% probability being within the brain were included).

2.2.2 Resting-state fMRI

For rs-fMRI, echoplanar imaging (EPI) acquired 261 volumes with 32 slices (sequential descending order, slice thickness of 3.7 mm with a slice gap of 20% for whole-brain coverage, TR = 1970 ms; TE = 30 ms; flip angle $\alpha = 78°$; FOV = 192 mm × 192 mm; resolution = 3 mm × 3 mm × 4.44 mm) during 8 min and 40 s. Participants were instructed to lie still with their eyes closed. The initial six volumes were discarded to allow for T1 equilibration. The imaging data were analyzed using Automatic Analysis (Cusack et al., 2014) calling functions from SPM12, as described previously (Tsvetanov et al., 2016).

Rs-fMRI data were further processed using whole-brain ICA of single-subject time series denoising, with noise components selected and removed automatically using the ICA-based Automatic Removal of Motion Artifacts toolbox (AROMA) (Pruim, Mennes, Buitelaar, & Beckmann, 2015; Pruim, Mennes, van Rooij, et al., 2015). This was complemented with linear detrending of the fMRI signal, covarying out six realignment parameters, white matter and cerebrospinal fluid signals, their first derivatives, and quadratic terms (Pruim, Mennes, van Rooij, et al., 2015). Global white matter and cerebrospinal fluid signals were estimated for each volume from the mean value of white matter and cerebrospinal fluid masks derived by thresholding SPM tissue probability maps at 0.75. Rs-fMRI data were head motion corrected, bandpass filtered and spatially smoothed with a 6 mm FWHM Gaussian kernel.

2.2.3 Cerebrovascular imaging

2.2.3.1 ASL

To assess resting cerebral blood flow, pulsed ASL was used (PASL, PICORE-Q2T-PASL in axial direction, 2,500 ms repetition time, 13 ms echo time, bandwidth 2,232 Hz/Px, 256 × 256 mm2 field of view, imaging matrix 64 × 64, 10 slices, 8 mm slice thickness, flip angle 90°, 700 ms TI1, TI2 = 1,800 ms, 1,600 ms saturation stop time). The imaging volume was positioned to maintain maximal brain coverage with a 20.9 mm gap between the imaging volume and a labeling slab with 100 mm thickness. There were 90 repetitions giving 45 control-tag pairs (duration 3'52"). A single-shot EPI (M0) equilibrium magnetization scan was acquired. Pulsed ASL time series were converted to cerebral blood flow maps using ExploreASL toolbox (Mutsaerts et al., 2018). Following rigid-body alignment, the images were coregistered with the T1 volume, normalised with normalization parameters from the T1 stream to warp ASL images into MNI space and smoothed with a 12 mm FWHM Gaussian kernel (Tsvetanov, Henson, Jones, et al., 2021).

2.2.3.2 Resting state fluctuation amplitude (RSFA)

An index of cerebrovascular reactivity was estimated using the resting state fluctuation amplitude (RSFA)(Kannurpatti & Biswal, 2008; Tsvetanov et al., 2015; Tsvetanov, Henson, & Rowe, 2021). RSFA was estimated from resting-state EPI as described in section 2.2.2 and smoothed with an 8 mm FWHM Gaussian kernel. Subject specific RSFA maps were calculated based on the normalized standard deviation across time for processed rs-fMRI time series data. Details on the acquisition and processing of RSFA are reported previously (Tsvetanov, Henson, Jones, et al., 2021).

2.3 Imaging analysis

2.3.1 Functional network decomposition using group-ICA

In order to identify functional networks from rs-fMRI and study network spatial patterns, an ICA was performed using the Group-level ICA of fMRI Toolbox to decompose the rs-fMRI (trendscenter.org/software/gift/)(V. D. Calhoun, Adali, Pearlson, & Pekar, 2001). ICA dissociates signals from complex datasets with minimal assumptions (V. Calhoun, 2018), to represent data in a small number of independent components (ICs) which here are spatial maps that describe

the temporal and spatial characteristics of underlying signals (V. D. Calhoun et al., 2001; McKeown et al., 1998). Each component can therefore be interpreted as similar BOLD activity of a functional network (Rosazza & Minati, 2011).

The data from participants in Cam-CAN Stage 2 (n = 648) were analyzed using ICA. This provided a twofold advantage: subjects excluded from the main analysis formed an independent validation sample (see below in 2.4); and having a larger sample increases the reliability of ICA decomposition results while maximizing statistical power (V. D. Calhoun, Kiehl, & Pearlson, 2008; Erhardt et al., 2011). The number of components used, N = 15, matched a common degree of decomposition previously applied in low-dimensional ICA of rs-fMRI (Beckmann, DeLuca, Devlin, & Smith, 2005; Damoiseaux et al., 2006; Smith et al., 2009) and generated network spatial maps that showed a high degree of overlapping with network templates. Low-dimensional ICA was used because the purpose was to define each network with a single component, and high-dimensional ICA would tend to decompose single network into multiple components. Hundred ICASSO iterations were used to ensure the reliability of estimated ICs (Himberg & Hyvarinen, 2003). Functional networks were identified from components by visualization and validated by spatially matching the components to pre-existing templates (Shirer, Ryali, Rykhlevskaia, Menon, & Greicius, 2012), in accordance with previous methodology used to identify networks from ICs (Tsvetanov et al., 2016).

2.3.2 Multimodal fusion using linked ICA

Linked ICA was performed using FLICA of FMRIB (https://fsl.fmrib.ox.ac.uk/fsl/fslwiki/FLICA) (Groves et al., 2011; Smith et al., 2004) implemented in Matlab (MathWorks version 2020b). Linked ICA was run with 7 spatial map inputs: T1 grey matter images, ASL, RSFA and four maps from three resting-state functional networks of those subjects that were included in Stage 3 (i.e., the DMN, the SN, the right FPN and the left FPN) (Day et al., 2013; Marek & Dosenbach, 2018; Rosazza & Minati, 2011; Zhou & Seeley, 2014). We refer to these imaging derived inputs as modalities. Within each modality, images from all subjects were concatenated into a single input image for linked ICA. To ensure that results were not influenced dominantly by non-grey

matter regions, a grey matter probability mask from SPM12 was used with a threshold of 0.3. We performed linked ICA using a dimensionality of 40, with 1000 iterations based on recommendation in previous studies (Doan, Engvig, Zaske, et al., 2017; Doan, Kaufmann, et al., 2017; Francx et al., 2016; Groves et al., 2012; Li et al., 2020; Wolfers et al., 2017). To ensure findings were robust to the model order, we also performed the linked ICA 30 and 50 dimensions.

2.4 Validation analysis in an independent Cam-CAN subset

To assess the reliability of fusion between neuroimaging modalities using the linked ICA toolbox, linked ICA was performed in an independent sample using the same processing steps and settings. This sample was a subset of the Cam-CAN cohort, comprised of participants who participated in Stage 2 (CC700) but were not included in the main analysis because they were either not selected to enter Stage 3 or had missing data from Stage 3 (CC280). This group, referred to as CC420, lacked ASL data so the linked ICA included 6 inputs only (DMN, SN, right FPN, left FPN, RSFA, T1). Other steps were the same as the main analysis (i.e., the acquisition and processing of neuroimaging data, functional network decomposition using group-ICA, and multimodal fusion using linked ICA).

2.5 Statistical analysis

Demographic variables were compared between age groups using one-way ANOVA for continuous variables and using chi-square test for categorical variable. Matching between functional network spatial maps and corresponding network templates was analyzed using simple correlation tests.

To investigate the relevance of linked ICA components with cognition, component subject loadings from linked ICA output were analyzed using multiple linear regression with robust fitting algorithm (Matlab function fitlm.m). Fluid intelligence was selected as a principal cognitive measure due to its broad positive correlations with other cognitive tests, and

sensitivity to age. Standard Cattell total score was used as a main indication of cognition in this study (Cattell, 1971; Cattell, Cattell, Institute for, & Ability, 1960; Shafto et al., 2014).

To investigate the association of linked ICA output components with Cattell score and other variates, Cattell score was used as the independent variable with age, gender and head motion as covariates in linear regression analysis. Each linked ICA component subject loading was used as the dependent variable. The overall model fit was corrected for multiple comparison using the Bonferroni correction of family-wise error rate (FWER). A corrected $P < 0.05$ was chosen as the significance level. Only those models with significant overall model fit after FWER-correction were considered as relevant in this study. To investigate whether there were components explained by shared variance between age and Cattell but not by the covariate on its own, commonality analysis (Nimon & Reio, 2011) between age and Cattell was performed with 10,000 permutations following the multiple linear regression. All statistical analyses were performed in Matlab version 2020b.

3. RESULTS

3.1 Characteristics of participants

Participants with imaging data from all modalities (i.e., rs-fMRI, ASL, RSFA, T1) were included, except those with image artefacts that could not be resolved (n = 25). The final analytic sample for the main analysis (CC280) included 215 subjects. The validation analysis sample (CC420) included 433 subjects. The demographic characteristics of participants are reported in **Table 1**.

3.2 Functional network decomposition using group-ICA

Among the 15 components generated from ICA, whole brain spatial maps associated with the following networks of interest specified a priori were identified: the DMN, the SN, and the lateralized FPNs (**Figure 2**). The correlation between each functional network spatial map and its corresponding template from a previous study (Shirer et al., 2012) was r = 0.62 for the DMN, r = 0.58 for the SN, r = 0.55 for the right FPN, and r = 0.54 for the left FPN.

Table 1. Characteristics of participants.

		Age range							Difference between deciles (ANOVA or χ^2)
	All	**18-27**	**28-37**	**38-47**	**48-57**	**58-67**	**68-77**	**78-88**	***P*-values**
CC280									
n	215	17	38	36	35	38	26	25	
Mean age (years)	52.9	24.6	33.5	43.6	52.2	62.8	72.3	81.0	
Gender *n* (%)									0.99
Males	106 (49.3)	7 (41.2)	19 (50)	19 (52.8)	18 (51.4)	19 (50)	12 (46.2)	12 (48)	
Females	109 (50.7)	10 (58.8)	19 (50)	17 (47.2)	17 (48.6)	19 (50)	14 (53.8)	13 (52)	
Cattell score									< 0.0001
Mean ± SD	33.5±6.0	37.8±4.4	38.4±4.5	35.5±3.8	33.6±4.5	32.2±5.0	28.9±4.2	26.4±5.7	
Mini-Mental State Examination									0.0099
Mean ± SD	29.2±1.0	29.3±0.9	29.7±0.6	29.1±1.2	29.3±0.8	29.1±1.0	29.0±1.2	28.7±1.4	
CC420									
n	433	34	66	62	64	62	75	70	
Mean age (years)	55.1	22.8	32.4	42.5	52.5	62.3	72.1	81.3	
Gender *n* (%)									0.98
Males	212 (49.0)	16 (47.1)	31 (47.0)	28 (45.2)	31 (48.4)	31 (50.0)	38 (50.7)	37 (52.9)	
Females	221 (51.0)	18 (52.9)	35 (53.0)	34 (54.8)	33 (51.6)	31 (50.0)	37 (49.3)	33 (47.1)	
Cattell score									< 0.0001
Mean ± SD	31.0±7.0	37.3±3.7	36.5±4.0	34.9±4.5	33.4±4.6	29.6±5.3	26.4±6.2	23.5±5.6	
Mini-Mental State Examination									< 0.0001
Mean ± SD	28.8±1.3	29.1±1.5	29.4±1.1	29.1±1.1	29.1±1.2	29.0±1.2	28.4±1.3	27.9±1.5	

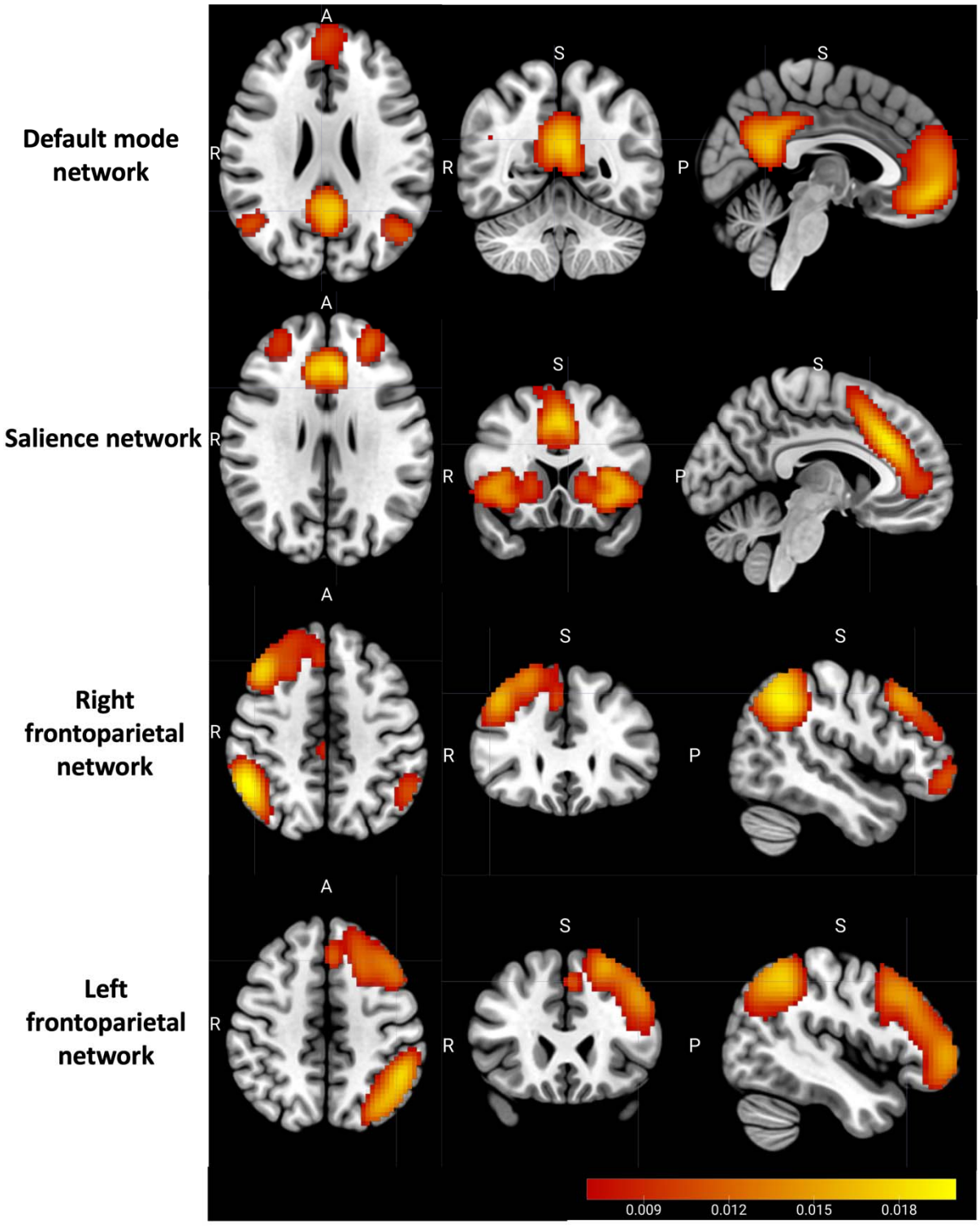

Figure 2. The spatial maps associated with the default mode network, the salience network, and the lateralized frontoparietal networks, generated from independent component analysis of 648 subjects from Cam-CAN cohort Stage 2.

3.3 Multimodal fusion using linked ICA

The relative weight of modalities in each component is shown in **Figure 3a**. Only modalities with significant voxel values (i.e., *t*-score > 3.34 which corresponds to $p < 0.001$) are presented. Two components with no significant subject loadings from any modality were excluded. Most components (> 75%) were dominated by a single input neuroimaging modality. Components reflecting structural and cerebrovascular inputs explained overall more variance compared to resting-state functional network topography. Fusion between imaging inputs were observed between T1, ASL and RSFA maps (i.e., IC4, IC14, IC33). Fusion was also observed between different functional networks (i.e., IC19, IC24, IC26, IC38). However, no fusion was observed between functional network, cerebrovascular and structural spatial maps. Linked ICA was repeated with different numbers of components in order to ensure the results were not significantly affected by the ICA dimensionality. Fusion patterns between modalities shown in linked ICA with 30, 40, and 50 components, respectively, are summarized in **Figure 4**.

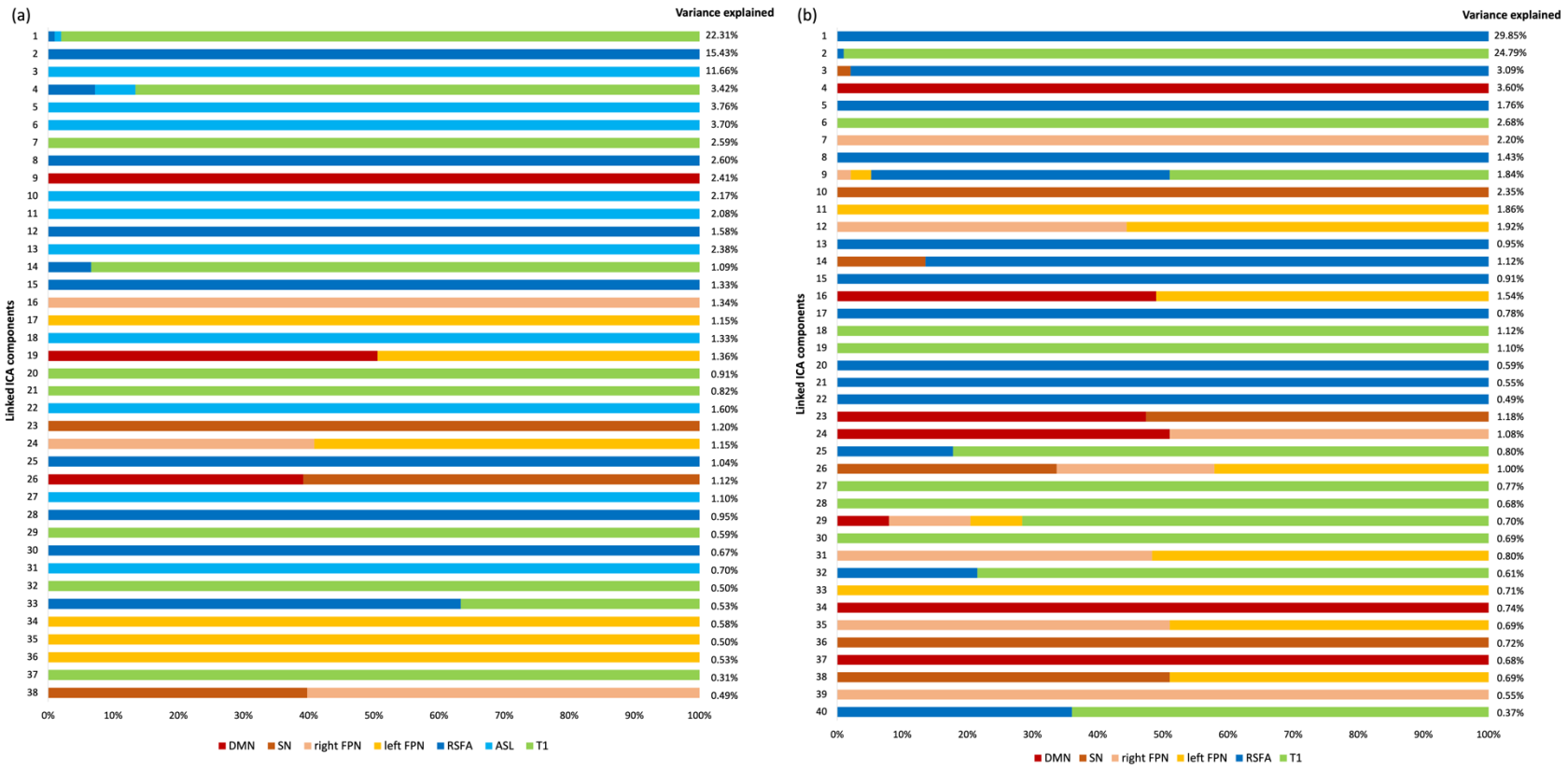

Figure 3. The relative weight of modalities in each component generated from linked ICA and the percentage of variance explained of each component of the (a) CC280 participants (*n* = 215), and (b) CC420 participants (*n* = 433). Note that most components are dominated by one modality. Abbreviations: DMN, default mode network; SN, salience network; FPN, frontoparietal network; RSFA, resting state fluctuation amplitude; ASL, arterial spin labelling.

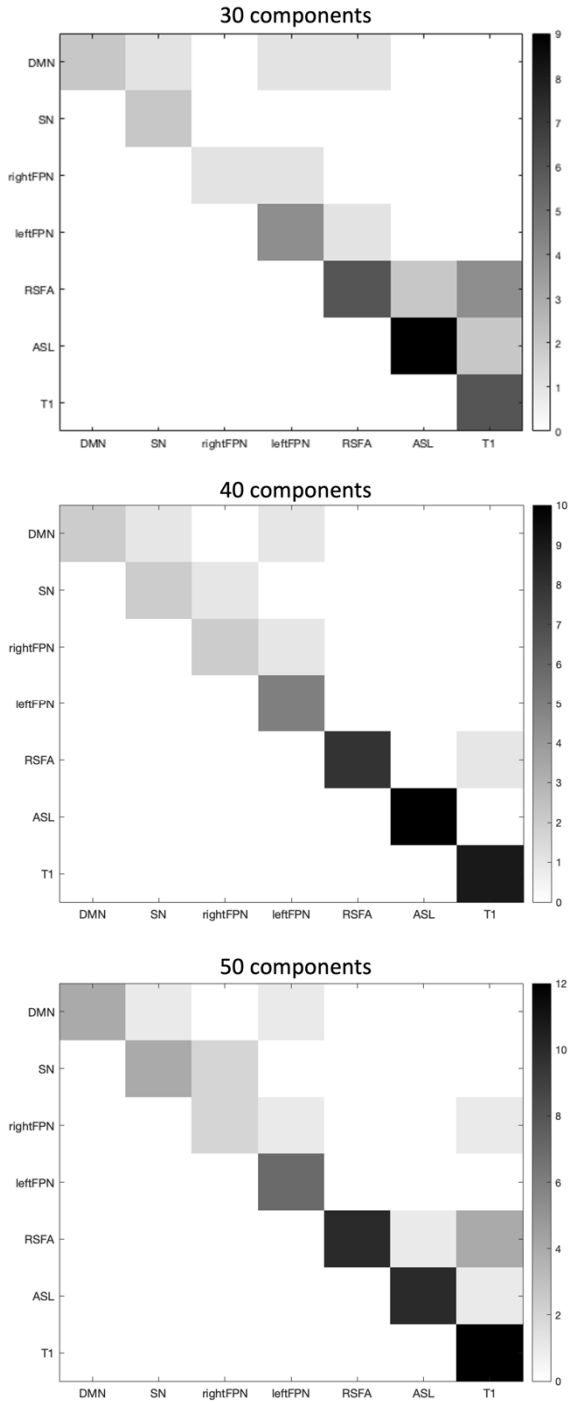

Figure 4. Degree of fusion between the 7 neuroimaging modalities included in linked ICA CC280 (*n* = 215) with 30, 40, and 50 components, respectively. Greater number (i.e., darker color) in the matrix represents more fusion found between the two modalities in linked ICA output components. Abbreviations: DMN, default mode network; SN, salience network; FPN, frontoparietal network; RSFA, resting state fluctuation amplitude; ASL, arterial spin labelling.

3.4 Age- and behaviour-related effects on linked ICA subject loadings

Results of linear regression analysis with age and cognition are shown in **Table 2**. The overall model fits of 16 components remained significant after FWER-correction. Among these 16 components, Cattell score was significantly correlated with IC1 which reflected global grey matter atrophy with regional ASL and RSFA signals (**Figure 5a**), adjusting for age, gender and head motion covariates. Cattell score correlated with IC16 which reflected right FPN signals (**Figure 5a**) and IC17 which reflected the left FPN signals. IC1, IC4, IC13, IC15, IC16, IC17, IC19, IC23, IC25, IC26, IC27 and IC33 showed shared variance between age and Cattell score, suggesting age-related differences in cognitive performance indicated by fluid intelligence.

Table 2. Linear regression analysis results of the independent component (IC) subject loading from linked independent component analysis (7 modalities) of CC280 participants (n = 215), followed by common variance analysis between age and Cattell in predicting IC.

	IC ~ Cattell + age + gender + head motion							Common variance between age and Cattell	
IC	Overall model fit			Age		Cattell			
	Adjusted R^2	P	FWER-corrected P	t	P	t	P	R^2	P
IC1	0.56	< 0.0001	**< 0.0001**	-8.44	**< 0.0001**	2.79	**0.0058**	0.17	**< 0.0001**
IC2	0.016	0.12	> 0.99						
IC3	0.0053	0.28	> 0.99						
IC4	0.69	< 0.0001	**< 0.0001**	11.52	**< 0.0001**	1.43	0.15	0.056	**< 0.0001**
IC5	0.0051	0.28	> 0.99						
IC6	0.17	< 0.0001	**< 0.0001**	-2.45	**0.015**	-1.22	0.23	-0.0055	0.10
IC7	0.033	0.026	> 0.99						
IC8	0.0031	0.33	> 0.99						
IC9	0.056	0.0029	0.12						
IC10	0.024	0.060	> 0.99						
IC11	0.021	0.074	> 0.99						
IC12	-0.0051	0.58	> 0.99						
IC13	0.097	< 0.0001	**0.0016**	-2.64	**0.0090**	0.39	0.70	0.022	**0.0024**
IC14	0.036	0.019	0.76						
IC15	0.27	< 0.0001	**< 0.0001**	2.71	**0.0073**	-1.41	0.16	0.038	**0.0001**
IC16	0.15	< 0.0001	**< 0.0001**	-0.83	0.41	2.87	**0.0045**	0.034	**0.0003**

IC17	0.15	< 0.0001	**< 0.0001**	0.48	0.63	3.10	**0.0022**	0.0092	**0.044**
IC18	0.10	< 0.0001	**0.00098**	-3.12	**0.0021**	-0.54	0.59	0.0087	0.050
IC19	0.065	0.0012	**0.048**	2.51	**0.013**	-0.78	0.44	0.030	**0.0006**
IC20	0.046	0.0073	0.29						
IC21	0.073	0.00053	**0.021**	-0.071	0.94	0.65	0.51	0.0013	0.30
IC22	0.088	0.00011	**0.0044**	-2.34	**0.020**	-0.56	0.58	0.0027	0.20
IC23	0.12	< 0.0001	**< 0.0001**	-2.04	**0.043**	0.13	0.89	0.010	**0.030**
IC24	0.055	0.0030	0.12						
IC25	0.12	< 0.0001	**< 0.0001**	-2.74	**0.0068**	0.0082	0.99	0.015	**0.0088**
IC26	0.18	< 0.0001	**< 0.0001**	-1.91	0.058	1.68	0.094	0.034	**0.0001**
IC27	0.068	0.00084	**0.034**	-1.20	0.23	0.61	0.54	0.0095	**0.041**
IC28	0.059	0.0021	0.084						
IC29	0.0071	0.24	> 0.99						
IC30	0.040	0.014	0.56						
IC31	0.053	0.0040	0.16						
IC32	0.058	0.0024	0.096						
IC33	0.064	0.0012	**0.048**	-3.31	**0.0011**	-0.27	0.79	0.017	**0.0072**
IC34	0.028	0.040	> 0.99						
IC35	0.030	0.035	> 0.99						
IC36	-0.013	0.86	> 0.99						
IC37	0.0052	0.28	> 0.99						
IC38	0.019	0.0089	0.36						

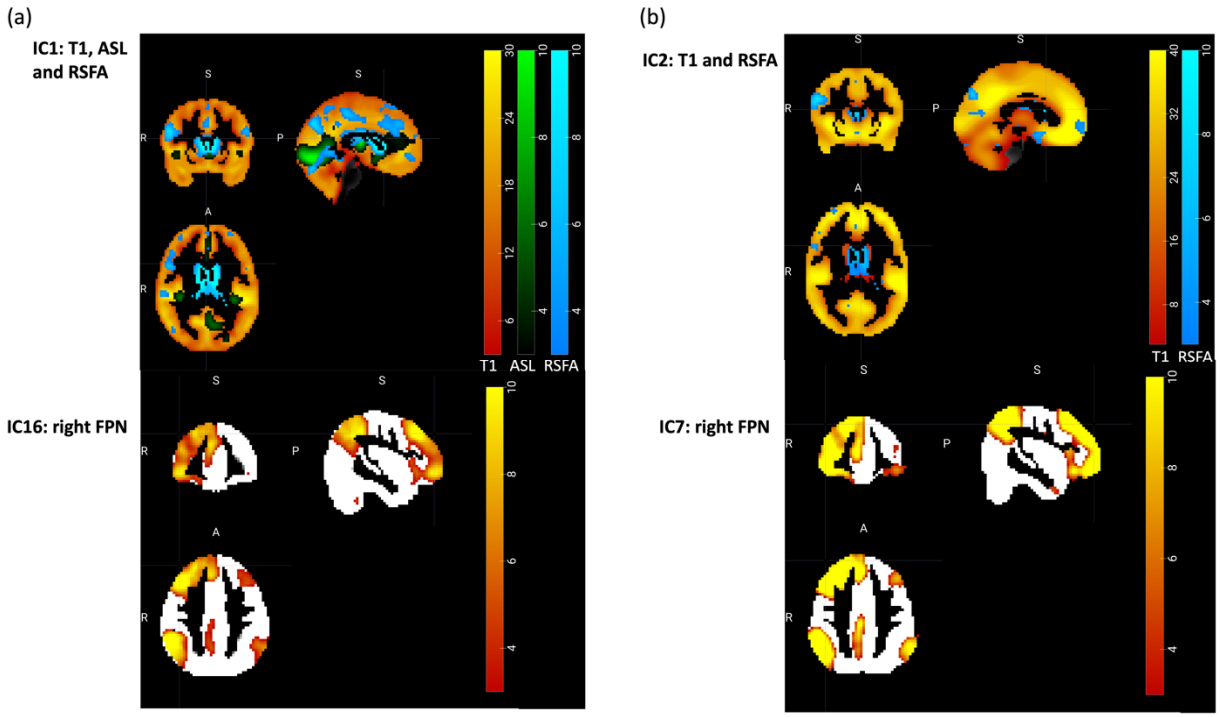

Figure 5. Components that were significantly associated with fluid intelligence over and above age and gender. (a) CC280 participants (n = 215): spatial maps of linked ICA output component 1 (IC1) which reflects the subject loading of T1, arterial spin labelling (ASL) and resting state fluctuation amplitude (RSFA); and component 16 (IC16) which reflects the subject loading of the right frontoparietal network (FPN). For visualization the threshold is set to $3 < Z < 30$ for T1, $3 < Z < 10$ for ASL and RSFA in IC1; and $3 < Z < 10$ in IC16. (b) CC420 participants (n = 433): spatial maps of linked ICA output component 2 (IC2) which reflects the subject loading of T1 and RSFA, and component 7 (IC7) which reflects the subject loading of the right FPN. For visualization the threshold is set to $3 < Z < 40$ for T1 and $3 < Z < 10$ for RSFA in IC2, and $3 < Z < 10$ in IC7.

3.5 Validation analysis in an independent Cam-CAN subset

CC420 results were consistent with those of CC280 sample. The relative weight of modalities in each linked ICA output component is shown in **Figure 3b**. Only modalities with significant voxel values (i.e., $t > 3.34$) are presented.

Results of linear regression analysis are shown in **Table 3**. The overall model fits of 19 components remained significant after FWER-correction and therefore these components were

considered as relevant in this study. Models that were not significant after FWER-correction were considered as components related to noise signals but not related to the predictors in the models. Among the 19 relevant components, including age, gender and head motion as covariates and correcting for multiple comparisons, Cattell score was significantly correlated with IC2 which reflected global grey matter atrophy with regional RSFA signals (**Figure 5b**) and this component was similar to IC1 in CC280 analysis. Cattell score was significantly correlated with IC7 which reflected right FPN signals (**Figure 5b**), and this component was similar to IC16 in CC280 analysis. Cattell score was also significantly correlated with IC10 which reflected the SN signals.

Table 3. Linear regression analysis results of the validation analysis of the independent component (IC) subject loading from linked independent component analysis (6 modalities) of CC420 (*n* = 433), followed by common variance analysis between age and Cattell in predicting IC.

	IC ~ Cattell + age + gender + head motion							Common variance between age and Cattell	
IC	Overall model fit			Age		Cattell			
	Adjusted R^2	*P*	FWER-corrected *P*	t	*P*	t	*P*	R^2	*P*
IC1	0.14	< 0.0001	**< 0.0001**	-6.22	**< 0.0001**	-0.27	0.79	0.036	**< 0.0001**
IC2	0.43	< 0.0001	**< 0.0001**	-7.03	**< 0.0001**	3.72	**0.00023**	0.12	**< 0.0001**
IC3	0.043	0.00021	**0.0084**	-2.64	**0.0086**	0.92	0.36	0.029	**0.0001**
IC4	0.0077	0.13	> 0.99						
IC5	0.28	< 0.0001	**< 0.0001**	3.50	**0.00051**	-1.75	0.082	0.046	**< 0.0001**
IC6	0.053	< 0.0001	**0.0011**	-1.30	0.19	0.10	0.92	0.00079	0.30
IC7	0.26	< 0.0001	**< 0.0001**	-2.63	**0.0088**	2.64	**0.0087**	0.046	**< 0.0001**
IC8	0.00036	0.39	> 0.99						
IC9	0.66	< 0.0001	**< 0.0001**	-17.92	**< 0.0001**	1.59	0.11	0.23	**< 0.0001**
IC10	0.26	< 0.0001	**< 0.0001**	-3.75	**0.00021**	2.05	**0.041**	0.061	**< 0.0001**
IC11	0.18	< 0.0001	**< 0.0001**	-2.35	**0.019**	0.88	0.38	0.018	**0.0002**
IC12	-0.0033	0.62	> 0.99						
IC13	-0.0042	0.68	> 0.99						
IC14	0.22	< 0.0001	**< 0.0001**	-2.86	**0.0044**	-1.93	0.054	-0.0047	0.061

IC15	0.0070	0.14	> 0.99						
IC16	0.020	0.016	0.64						
IC17	0.067	< 0.0001	**< 0.0001**	-3.54	**0.00045**	-0.023	0.98	0.014	**0.0013**
IC18	0.025	0.0065	0.26						
IC19	0.13	< 0.0001	**< 0.0001**	-0.13	0.90	1.38	0.17	0.0026	0.13
IC20	0.043	0.00018	**0.0072**	-0.96	0.34	-1.96	0.051	-0.0018	0.19
IC21	0.050	< 0.0001	**0.0021**	2.68	**0.0076**	0.31	0.75	0.0089	**0.011**
IC22	0.050	< 0.0001	**0.0021**	2.01	**0.045**	-1.40	0.16	0.027	**< 0.0001**
IC23	0.11	< 0.0001	**< 0.0001**	-4.74	**< 0.0001**	-0.71	0.48	0.027	**< 0.0001**
IC24	-0.00067	0.45	> 0.99						
IC25	0.0096	0.093	> 0.99						
IC26	0.093	< 0.0001	**< 0.0001**	4.11	**< 0.0001**	-0.22	0.83	0.024	**< 0.0001**
IC27	0.014	0.044	> 0.99						
IC28	0.027	0.0044	0.18						
IC29	-0.0047	0.72	> 0.99						
IC30	0.047	< 0.0001	**0.0036**	-0.55	0.58	-1.18	0.24	-0.00047	0.36
IC31	0.011	0.068	> 0.99						
IC32	-0.0077	0.93	> 0.99						
IC33	0.0023	0.29	> 0.99						
IC34	0.13	< 0.0001	**< 0.0001**	2.45	**0.015**	-0.20	0.84	0.012	**0.0024**
IC35	0.0071	0.14	> 0.99						
IC36	0.0046	0.21	> 0.99						
IC37	-0.0026	0.57	> 0.99						
IC38	-0.0087	0.98	> 0.99						
IC39	-0.0041	0.68	> 0.99						
IC40	-0.0040	0.67	> 0.99						

4. DISCUSSION

In the current study, multivariate data-driven analysis characterized the patterns of structural and functional change in the brain across the adult lifespan in two sets of healthy subjects from 18 – 88 years old. There was evidence for concordant changes in morphometry and cerebrovascular signals, but not between resting-state network spatial maps and morphometry

or cerebrovascular signals. The age-related variance in expression of few linked ICA components was cognitively relevant. In particular, the joint changes in diffuse brain atrophy with regional cerebrovascular changes and the right FPN activity correlated with fluid intelligence over and above age and gender. The principal findings were replicated in the second cohort. We propose that multimodal integration allows to better characterize structural and functional brain changes of healthy ageing.

The linked ICA identified a strong effect of global grey matter atrophy, in IC1 from the main analysis and IC2 from the validation analysis. This is consistent with previous studies of ageing using linked ICA (Doan, Engvig, Zaske, et al., 2017; Douaud et al., 2014). Cerebrovascular measures were identified in the same component, suggesting that the atrophy effects were partly linked to cerebrovascular health. This accords with large-scale lifespan studies showing global brain atrophy association with cerebrovascular changes (Asllani et al., 2009; Iadecola, 2017; Kennedy & Raz, 2015; Lemaitre et al., 2012; Peelle, Cusack, & Henson, 2012).

Significant correlation between Cattell score and right FPN activity was observed in the main analysis and the validation analysis. The FPN is an important control network, in which functional integration is positively correlated with cognitive ability (Marek & Dosenbach, 2018; Sheffield et al., 2015). The current results are compatible with previous reports that the across-network connectivity of resting-state FPN is positively correlated with fluid intelligence (Bethlehem et al., 2020; Cole, Ito, & Braver, 2015; Hearne, Mattingley, & Cocchi, 2016).

In contrast with atrophy and cerebrovascular indices, there was little fusion between resting-state functional networks and other modalities (Maglanoc et al., 2020). In other words, the topography of resting-state functional networks was not matched to the topography of cerebrovascular or structural neuroimaging signals in independent components. However, the activity of the right FPN functional network correlated with fluid intelligence over and above age and gender. In contrast, in components reflecting signals from the DMN (IC19, IC26), the SN (IC23, IC26), and the left FPN (IC17, IC19), there was common variance between age and Cattell

score in predicting the IC subject loading. This suggests that the network components reflected age-related differences in fluid intelligence.

The main advantage of linked ICA is its ability to combine imaging modalities with different spatial dimensions or features by applying ICA on each modality while accounting for the spatial correlation of each modality, enabling us to model shared variance across different imaging modalities (Groves et al., 2011; Groves et al., 2012). Hence, the derived components may be more sensitive to an effect of interest especially when the effect is present across different imaging modalities (Francx et al., 2016). Linked ICA has revealed morphological patterns that are related to age, cognition, and Alzheimer's disease (Alnaes et al., 2018; Doan, Engvig, Persson, et al., 2017; Doan, Engvig, Zaske, et al., 2017; Douaud et al., 2014; Groves et al., 2012) and predicted brain morphological patterns in neuropsychiatric disorders such as depression (Maglanoc et al., 2020), schizophrenia (Brandt et al., 2015; Doan, Kaufmann, et al., 2017), bipolar disorders (Doan, Kaufmann, et al., 2017), and attention-deficit/hyperactivity disorder (ADHD) (Francx et al., 2016). However, many previous studies using linked ICA focused on co-modelling brain structural effects across modalities, for example combining only grey matter morphological measures (e.g. grey matter density, cortical thickness) or combining grey with white matter properties (Doan, Engvig, Zaske, et al., 2017; Doan, Kaufmann, et al., 2017; Douaud et al., 2014; Francx et al., 2016). Here we showed the potential to characterize joint changes in functional, cerebrovascular and structural measures and disentangle their relationships with cognition and ageing.

We found no cognitively relevant fusion between functional network spatial maps and structural or cerebrovascular spatial maps. The majority of components were dominated by a single neuroimaging measurement. It suggests that variability of brain patterns in healthy ageing subjects is better characterized by multiple independent components dominated by one of the structural, cerebrovascular or functional network measurements, but not captured in a single component reflecting all of these signals. It also showed that in this sample of healthy participants, global grey matter atrophy and the right FPN activity were the dominant

components correlated with fluid intelligence. Although global atrophy was largely typical of ageing effects, by decomposing this dominant atrophy component from other components using linked ICA, it was possible to identify subtle effects across multiple imaging modalities which might otherwise be overlooked using other analysis approaches.

There are limitations in the present study. First, there is no standard dimensionality to be used in ICA. However, the number of components used in ICA and linked ICA in the present study was based on the most stable and favorable dimensionality indicated by previous literature (Beckmann et al., 2005; Damoiseaux et al., 2006; Doan, Engvig, Zaske, et al., 2017; Doan, Kaufmann, et al., 2017; Francx et al., 2016; Groves et al., 2012). Moreover, linked ICA was repeated with several dimensionalities and the results were similar: the fusion patterns in the derived components were similar and the cognitively relevant components were consistent across analyses with 30, 40 and 50 dimensions. Second, the Cattell test, which quantifies fluid intelligence, informed components with behavioural relevance. Future research could investigate more detailed or domain-specific brain-behavior relationships, for example by using specific cognitive tests which might enable us to dissociate domain-general from domain-specific associations. Third, the functional network spatial maps used in linked ICA were based on associations of components with the topography of functional networks. As joint consideration of activity and connectivity might better characterize the brain dynamics and cognitive performance in normal ageing (Tsvetanov et al., 2018), it is possible that connectivity between functional nodes could indicate more information than the functional network topography alone. Future research could consider investigating the intercorrelations between functional connectivity and multiple neuroimaging modalities.

5. CONCLUSION

We demonstrate the insights from linked ICA to bring together measurements from multimodal neuroimaging with their independent and additive information. We propose that using linked ICA to integrate multiple neuroimaging modalities allows to better characterize brain pattern

variability and to differentiate brain changes in healthy ageing. Across the lifespan, the most significant predictors of differences in fluid intelligence are global grey matter atrophy and right FPN activity. Linked ICA may provide new insights into the relative brain structural, functional and vascular contributors to cognitive impairment in disorders associated with ageing, including dementia and other neurodegenerative disease.

REFERENCES

Alnaes, D., Kaufmann, T., Doan, N. T., Cordova-Palomera, A., Wang, Y., Bettella, F., . . . Westlye, L. T. (2018). Association of Heritable Cognitive Ability and Psychopathology With White Matter Properties in Children and Adolescents. *JAMA Psychiatry, 75*(3), 287-295. doi:10.1001/jamapsychiatry.2017.4277

Asllani, I., Habeck, C., Borogovac, A., Brown, T. R., Brickman, A. M., & Stern, Y. (2009). Separating function from structure in perfusion imaging of the aging brain. *Hum Brain Mapp, 30*(9), 2927-2935. doi:10.1002/hbm.20719

Beard, J. R., Officer, A., de Carvalho, I. A., Sadana, R., Pot, A. M., Michel, J. P., . . . Chatterji, S. (2016). The World report on ageing and health: a policy framework for healthy ageing. *Lancet, 387*(10033), 2145-2154. doi:10.1016/S0140-6736(15)00516-4

Beckmann, C. F., DeLuca, M., Devlin, J. T., & Smith, S. M. (2005). Investigations into resting-state connectivity using independent component analysis. *Philos Trans R Soc Lond B Biol Sci, 360*(1457), 1001-1013. doi:10.1098/rstb.2005.1634

Bethlehem, R. A. I., Paquola, C., Seidlitz, J., Ronan, L., Bernhardt, B., Consortium, C. C., & Tsvetanov, K. A. (2020). Dispersion of functional gradients across the adult lifespan. *Neuroimage, 222*, 117299. doi:10.1016/j.neuroimage.2020.117299

Brandt, C. L., Doan, N. T., Tonnesen, S., Agartz, I., Hugdahl, K., Melle, I., . . . Westlye, L. T. (2015). Assessing brain structural associations with working-memory related brain patterns in schizophrenia and healthy controls using linked independent component analysis. *Neuroimage Clin, 9*, 253-263. doi:10.1016/j.nicl.2015.08.010

Calhoun, V. (2018). Data-driven approaches for identifying links between brain structure and function in health and disease. *Dialogues Clin Neurosci, 20*(2), 87-99.

Calhoun, V. D., Adali, T., Pearlson, G. D., & Pekar, J. J. (2001). A method for making group inferences from functional MRI data using independent component analysis. *Hum Brain Mapp, 14*(3), 140-151. doi:10.1002/hbm.1048

Calhoun, V. D., Kiehl, K. A., & Pearlson, G. D. (2008). Modulation of temporally coherent brain networks estimated using ICA at rest and during cognitive tasks. *Hum Brain Mapp, 29*(7), 828-838. doi:10.1002/hbm.20581

Cattell, R. B. (1971). *Abilities : their structure, growth, and action [by] Raymond B. Cattell*. Boston: Houghton Mifflin.

Cattell, R. B., Cattell, A. K. S., Institute for, P., & Ability, T. (1960). *Measuring intelligence with the Culture Fair Tests*. Champaign, Ill.: Institute for Personality and Ability Testing.

Chen, J. E., & Glover, G. H. (2015). Functional Magnetic Resonance Imaging Methods. *Neuropsychol Rev, 25*(3), 289-313. doi:10.1007/s11065-015-9294-9

Cole, M. W., Bassett, D. S., Power, J. D., Braver, T. S., & Petersen, S. E. (2014). Intrinsic and task-evoked network architectures of the human brain. *Neuron, 83*(1), 238-251. doi:10.1016/j.neuron.2014.05.014

Cole, M. W., Ito, T., & Braver, T. S. (2015). Lateral Prefrontal Cortex Contributes to Fluid Intelligence Through Multinetwork Connectivity. *Brain Connect, 5*(8), 497-504. doi:10.1089/brain.2015.0357

Corbetta, M., & Shulman, G. L. (2002). Control of goal-directed and stimulus-driven attention in the brain. *Nat Rev Neurosci, 3*(3), 201-215. doi:10.1038/nrn755

Cusack, R., Vicente-Grabovetsky, A., Mitchell, D. J., Wild, C. J., Auer, T., Linke, A. C., & Peelle, J. E. (2014). Automatic analysis (aa): efficient neuroimaging workflows and parallel processing using Matlab and XML. *Front Neuroinform, 8*, 90. doi:10.3389/fninf.2014.00090

Damoiseaux, J. S., Rombouts, S. A., Barkhof, F., Scheltens, P., Stam, C. J., Smith, S. M., & Beckmann, C. F. (2006). Consistent resting-state networks across healthy subjects. *Proc Natl Acad Sci U S A, 103*(37), 13848-13853. doi:10.1073/pnas.0601417103

Day, G. S., Farb, N. A., Tang-Wai, D. F., Masellis, M., Black, S. E., Freedman, M., . . . Chow, T. W. (2013). Salience network resting-state activity: prediction of frontotemporal dementia progression. *JAMA Neurol, 70*(10), 1249-1253. doi:10.1001/jamaneurol.2013.3258

Doan, N. T., Engvig, A., Persson, K., Alnaes, D., Kaufmann, T., Rokicki, J., . . . Westlye, L. T. (2017). Dissociable diffusion MRI patterns of white matter microstructure and connectivity in Alzheimer's disease spectrum. *Sci Rep, 7*, 45131. doi:10.1038/srep45131

Doan, N. T., Engvig, A., Zaske, K., Persson, K., Lund, M. J., Kaufmann, T., . . . Alzheimer's Disease Neuroimaging, I. (2017). Distinguishing early and late brain aging from the Alzheimer's disease spectrum: consistent morphological patterns across independent samples. *Neuroimage, 158*, 282-295. doi:10.1016/j.neuroimage.2017.06.070

Doan, N. T., Kaufmann, T., Bettella, F., Jorgensen, K. N., Brandt, C. L., Moberget, T., . . . Westlye, L. T. (2017). Distinct multivariate brain morphological patterns and their added predictive value with cognitive and polygenic risk scores in mental disorders. *Neuroimage Clin, 15*, 719-731. doi:10.1016/j.nicl.2017.06.014

Douaud, G., Groves, A. R., Tamnes, C. K., Westlye, L. T., Duff, E. P., Engvig, A., . . . Johansen-Berg, H. (2014). A common brain network links development, aging, and vulnerability to disease. *Proc Natl Acad Sci U S A, 111*(49), 17648-17653. doi:10.1073/pnas.1410378111

Erhardt, E. B., Rachakonda, S., Bedrick, E. J., Allen, E. A., Adali, T., & Calhoun, V. D. (2011). Comparison of multi-subject ICA methods for analysis of fMRI data. *Hum Brain Mapp, 32*(12), 2075-2095. doi:10.1002/hbm.21170

Fox, M. D., Snyder, A. Z., Vincent, J. L., Corbetta, M., Van Essen, D. C., & Raichle, M. E. (2005). The human brain is intrinsically organized into dynamic, anticorrelated functional networks. *Proc Natl Acad Sci U S A, 102*(27), 9673-9678. doi:10.1073/pnas.0504136102

Francx, W., Llera, A., Mennes, M., Zwiers, M. P., Faraone, S. V., Oosterlaan, J., . . . Beckmann, C. F. (2016). Integrated analysis of gray and white matter alterations in attention-deficit/hyperactivity disorder. *Neuroimage Clin, 11*, 357-367. doi:10.1016/j.nicl.2016.03.005

Grady, C. (2012). The cognitive neuroscience of ageing. *Nature Reviews Neuroscience, 13*(7), 491-505. doi:10.1038/nrn3256

Grajauskas, L. A., Siu, W., Medvedev, G., Guo, H., D'Arcy, R. C. N., & Song, X. (2019). MRI-based evaluation of structural degeneration in the ageing brain: Pathophysiology and assessment. *Ageing Res Rev, 49*, 67-82. doi:10.1016/j.arr.2018.11.004

Groves, A. R., Beckmann, C. F., Smith, S. M., & Woolrich, M. W. (2011). Linked independent component analysis for multimodal data fusion. *Neuroimage, 54*(3), 2198-2217. doi:10.1016/j.neuroimage.2010.09.073

Groves, A. R., Smith, S. M., Fjell, A. M., Tamnes, C. K., Walhovd, K. B., Douaud, G., . . . Westlye, L. T. (2012). Benefits of multi-modal fusion analysis on a large-scale dataset: life-span patterns of inter-subject variability in cortical morphometry and white matter microstructure. *Neuroimage, 63*(1), 365-380. doi:10.1016/j.neuroimage.2012.06.038

Hearne, L. J., Mattingley, J. B., & Cocchi, L. (2016). Functional brain networks related to individual differences in human intelligence at rest. *Scientific Reports, 6*(1), 32328. doi:10.1038/srep32328

Himberg, J., & Hyvarinen, A. (2003). Icasso: software for investigating the reliability of ICA estimates by clustering and visualization. *2003 IEEE XIII Workshop on Neural Networks for Signal Processing (IEEE Cat. No.03TH8718)*, 259-268.

Iadecola, C. (2017). The Neurovascular Unit Coming of Age: A Journey through Neurovascular Coupling in Health and Disease. *Neuron, 96*(1), 17-42. doi:10.1016/j.neuron.2017.07.030

Kannurpatti, S. S., & Biswal, B. B. (2008). Detection and scaling of task-induced fMRI-BOLD response using resting state fluctuations. *Neuroimage, 40*(4), 1567-1574. doi:10.1016/j.neuroimage.2007.09.040

Kelly, A. M., Uddin, L. Q., Biswal, B. B., Castellanos, F. X., & Milham, M. P. (2008). Competition between functional brain networks mediates behavioral variability. *Neuroimage, 39*(1), 527-537. doi:10.1016/j.neuroimage.2007.08.008

Kennedy, K. M., & Raz, N. (2015). Normal Aging of the Brain. In A. W. Toga (Ed.), *Brain Mapping* (pp. 603-617). Waltham: Academic Press.

Kisler, K., Nelson, A. R., Montagne, A., & Zlokovic, B. V. (2017). Cerebral blood flow regulation and neurovascular dysfunction in Alzheimer disease. *Nat Rev Neurosci, 18*(7), 419-434. doi:10.1038/nrn.2017.48

Lemaitre, H., Goldman, A. L., Sambataro, F., Verchinski, B. A., Meyer-Lindenberg, A., Weinberger, D. R., & Mattay, V. S. (2012). Normal age-related brain morphometric changes: nonuniformity across cortical thickness, surface area and gray matter volume? *Neurobiol Aging, 33*(3), 617 e611-619. doi:10.1016/j.neurobiolaging.2010.07.013

Li, H., Smith, S. M., Gruber, S., Lukas, S. E., Silveri, M. M., Hill, K. P., . . . Nickerson, L. D. (2020). Denoising scanner effects from multimodal MRI data using linked independent component analysis. *Neuroimage, 208*, 116388. doi:10.1016/j.neuroimage.2019.116388

Maglanoc, L. A., Kaufmann, T., Jonassen, R., Hilland, E., Beck, D., Landro, N. I., & Westlye, L. T. (2020). Multimodal fusion of structural and functional brain imaging in depression using

linked independent component analysis. *Hum Brain Mapp, 41*(1), 241-255. doi:10.1002/hbm.24802

Marek, S., & Dosenbach, N. U. F. (2018). The frontoparietal network: function, electrophysiology, and importance of individual precision mapping. *Dialogues Clin Neurosci, 20*(2), 133-140.

McKeown, M. J., Makeig, S., Brown, G. G., Jung, T. P., Kindermann, S. S., Bell, A. J., & Sejnowski, T. J. (1998). Analysis of fMRI data by blind separation into independent spatial components. *Hum Brain Mapp, 6*(3), 160-188.

Moguilner, S., Garcia, A. M., Perl, Y. S., Tagliazucchi, E., Piguet, O., Kumfor, F., . . . Ibanez, A. (2020). Dynamic brain fluctuations outperform connectivity measures and mirror pathophysiological profiles across dementia subtypes: A multicenter study. *Neuroimage, 225*, 117522. doi:10.1016/j.neuroimage.2020.117522

Murley, A. G., Coyle-Gilchrist, I., Rouse, M. A., Jones, P. S., Li, W., Wiggins, J., . . . Rowe, J. B. (2020). Redefining the multidimensional clinical phenotypes of frontotemporal lobar degeneration syndromes. *Brain, 143*(5), 1555-1571. doi:10.1093/brain/awaa097

Mutsaerts, H., Petr, J., Thomas, D. L., De Vita, E., Cash, D. M., van Osch, M. J. P., . . . investigators, G. (2018). Comparison of arterial spin labeling registration strategies in the multi-center GENetic frontotemporal dementia initiative (GENFI). *J Magn Reson Imaging, 47*(1), 131-140. doi:10.1002/jmri.25751

Nimon, K., & Reio, T. G. (2011). Regression Commonality Analysis: A Technique for Quantitative Theory Building. *Human Resource Development Review, 10*(3), 329-340. doi:10.1177/1534484311411077

Peelle, J. E., Cusack, R., & Henson, R. N. (2012). Adjusting for global effects in voxel-based morphometry: gray matter decline in normal aging. *Neuroimage, 60*(2), 1503-1516. doi:10.1016/j.neuroimage.2011.12.086

Perry, D. C., Brown, J. A., Possin, K. L., Datta, S., Trujillo, A., Radke, A., . . . Seeley, W. W. (2017). Clinicopathological correlations in behavioural variant frontotemporal dementia. *Brain, 140*(12), 3329-3345. doi:10.1093/brain/awx254

Pini, L., Pievani, M., Bocchetta, M., Altomare, D., Bosco, P., Cavedo, E., . . . Frisoni, G. B. (2016). Brain atrophy in Alzheimer's Disease and aging. *Ageing Res Rev, 30*, 25-48. doi:10.1016/j.arr.2016.01.002

Pruim, R. H. R., Mennes, M., Buitelaar, J. K., & Beckmann, C. F. (2015). Evaluation of ICA-AROMA and alternative strategies for motion artifact removal in resting state fMRI. *Neuroimage, 112*, 278-287. doi:10.1016/j.neuroimage.2015.02.063

Pruim, R. H. R., Mennes, M., van Rooij, D., Llera, A., Buitelaar, J. K., & Beckmann, C. F. (2015). ICA-AROMA: A robust ICA-based strategy for removing motion artifacts from fMRI data. *Neuroimage, 112*, 267-277. doi:10.1016/j.neuroimage.2015.02.064

Raichle, M. E., & Mintun, M. A. (2006). Brain work and brain imaging. *Annu Rev Neurosci, 29*, 449-476. doi:10.1146/annurev.neuro.29.051605.112819

Romanowski, C. A., & Wilkinson, I. D. (2011). Atrophy: When too much atrophy is too little brain. *Neuroradiology, 53 Suppl 1*, S133-139. doi:10.1007/s00234-011-0929-0

Rosazza, C., & Minati, L. (2011). Resting-state brain networks: literature review and clinical applications. *Neurol Sci, 32*(5), 773-785. doi:10.1007/s10072-011-0636-y

Rosen, B. R., & Savoy, R. L. (2012). fMRI at 20: has it changed the world? *Neuroimage, 62*(2), 1316-1324. doi:10.1016/j.neuroimage.2012.03.004

Sahakian, B. J. (2014). What do experts think we should do to achieve brain health? *Neurosci Biobehav Rev, 43*, 240-258. doi:10.1016/j.neubiorev.2014.04.002

Shafto, M. A., Tyler, L. K., Dixon, M., Taylor, J. R., Rowe, J. B., Cusack, R., . . . Cam, C. A. N. (2014). The Cambridge Centre for Ageing and Neuroscience (Cam-CAN) study protocol: a cross-sectional, lifespan, multidisciplinary examination of healthy cognitive ageing. *BMC Neurol, 14*, 204. doi:10.1186/s12883-014-0204-1

Sheffield, J. M., Repovs, G., Harms, M. P., Carter, C. S., Gold, J. M., MacDonald, A. W., 3rd, . . . Barch, D. M. (2015). Fronto-parietal and cingulo-opercular network integrity and cognition in health and schizophrenia. *Neuropsychologia, 73*, 82-93. doi:10.1016/j.neuropsychologia.2015.05.006

Shirer, W. R., Ryali, S., Rykhlevskaia, E., Menon, V., & Greicius, M. D. (2012). Decoding subject-driven cognitive states with whole-brain connectivity patterns. *Cereb Cortex, 22*(1), 158-165. doi:10.1093/cercor/bhr099

Smith, S. M., Fox, P. T., Miller, K. L., Glahn, D. C., Fox, P. M., Mackay, C. E., . . . Beckmann, C. F. (2009). Correspondence of the brain's functional architecture during activation and rest. *Proc Natl Acad Sci U S A, 106*(31), 13040-13045. doi:10.1073/pnas.0905267106

Smith, S. M., Jenkinson, M., Woolrich, M. W., Beckmann, C. F., Behrens, T. E., Johansen-Berg, H., . . . Matthews, P. M. (2004). Advances in functional and structural MR image analysis and implementation as FSL. *Neuroimage, 23 Suppl 1*, S208-219. doi:10.1016/j.neuroimage.2004.07.051

Sweeney, M. D., Kisler, K., Montagne, A., Toga, A. W., & Zlokovic, B. V. (2018). The role of brain vasculature in neurodegenerative disorders. *Nat Neurosci, 21*(10), 1318-1331. doi:10.1038/s41593-018-0234-x

Taylor, J. R., Williams, N., Cusack, R., Auer, T., Shafto, M. A., Dixon, M., . . . Henson, R. N. (2017). The Cambridge Centre for Ageing and Neuroscience (Cam-CAN) data repository: Structural and functional MRI, MEG, and cognitive data from a cross-sectional adult lifespan sample. *Neuroimage, 144*(Pt B), 262-269. doi:10.1016/j.neuroimage.2015.09.018

Tibon, R., Tsvetanov, K. A., Price, D., Nesbitt, D., Can, C., & Henson, R. (2021). Transient neural network dynamics in cognitive ageing. *Neurobiol Aging, 105*, 217-228. doi:10.1016/j.neurobiolaging.2021.01.035

Tsvetanov, K. A., Gazzina, S., Jones, P. S., van Swieten, J., Borroni, B., Sanchez-Valle, R., . . . Genetic Ftd Initiative, G. (2021). Brain functional network integrity sustains cognitive function despite atrophy in presymptomatic genetic frontotemporal dementia. *Alzheimers Dement, 17*(3), 500-514. doi:10.1002/alz.12209

Tsvetanov, K. A., Henson, R. N., Tyler, L. K., Davis, S. W., Shafto, M. A., Taylor, J. R., . . . Rowe, J. B. (2015). The effect of ageing on fMRI: Correction for the confounding effects of vascular reactivity evaluated by joint fMRI and MEG in 335 adults. *Hum Brain Mapp, 36*(6), 2248-2269. doi:10.1002/hbm.22768

Tsvetanov, K. A., Henson, R. N., Tyler, L. K., Razi, A., Geerligs, L., Ham, T. E., . . . Neuroscience. (2016). Extrinsic and Intrinsic Brain Network Connectivity Maintains Cognition across the

Lifespan Despite Accelerated Decay of Regional Brain Activation. *J Neurosci, 36*(11), 3115-3126. doi:10.1523/JNEUROSCI.2733-15.2016

Tsvetanov, K. A., Henson, R. N. A., Jones, P. S., Mutsaerts, H., Fuhrmann, D., Tyler, L. K., . . . Rowe, J. B. (2021). The effects of age on resting-state BOLD signal variability is explained by cardiovascular and cerebrovascular factors. *Psychophysiology, 58*(7), e13714. doi:10.1111/psyp.13714

Tsvetanov, K. A., Henson, R. N. A., & Rowe, J. B. (2021). Separating vascular and neuronal effects of age on fMRI BOLD signals. *Philos Trans R Soc Lond B Biol Sci, 376*(1815), 20190631. doi:10.1098/rstb.2019.0631

Tsvetanov, K. A., Ye, Z., Hughes, L., Samu, D., Treder, M. S., Wolpe, N., . . . Neuroscience. (2018). Activity and Connectivity Differences Underlying Inhibitory Control Across the Adult Life Span. *J Neurosci, 38*(36), 7887-7900. doi:10.1523/JNEUROSCI.2919-17.2018

Wolfers, T., Arenas, A. L., Onnink, A. M. H., Dammers, J., Hoogman, M., Zwiers, M. P., . . . Beckmann, C. F. (2017). Refinement by integration: aggregated effects of multimodal imaging markers on adult ADHD. *J Psychiatry Neurosci, 42*(6), 386-394. doi:10.1503/jpn.160240

Zhou, J., & Seeley, W. W. (2014). Network dysfunction in Alzheimer's disease and frontotemporal dementia: implications for psychiatry. *Biol Psychiatry, 75*(7), 565-573. doi:10.1016/j.biopsych.2014.01.020